MGS Radio Science electron density profiles: Interannual variability and implications for the Martian neutral atmosphere

S. W. Bougher,[1] S. Engel,[2] D. P. Hinson,[3] and J. R. Murphy[4]

[1]   Martian electron density profiles provided by the Mars Global Surveyor (MGS) Radio Science (RS) experiment over the 95–200 km altitude range indicate wthat the height of the electron peak and the longitudinal structure of the peak height are sensitive indicators of the physical state of the Mars lower and upper atmospheres. The present analysis is carried out on five sets of occultation profiles, all at high solar zenith angles (SZA). Variations spanning 2 Martian years are investigated near aphelion conditions at high northern latitudes (64.7–77.6N) making use of four of these data sets. A mean ionospheric peak height of 133.5–135 km is obtained near SZA = 78–82°; a corresponding mean peak density of $7.3–8.5 \times 10^4$ cm^{-3} is also measured during solar moderate conditions at Mars. Strong wave number 2–3 oscillations in peak heights are consistently observed as a function of longitude over the 2 Martian years. These observed ionospheric features are remarkably similar during aphelion conditions 1 Martian year apart. This year-to-year repeatability in the thermosphere-ionosphere structure is consistent with that observed in multiyear aphelion temperature data of the Mars lower atmosphere [*Clancy et al.*, 2000; *Smith*, 2004]. Coupled Mars general circulation model (MGCM) and Mars thermospheric general circulation model (MTGCM) codes are run for Mars aphelion conditions, yielding mean and longitude variable ionospheric peak heights that reasonably match RS observations. A tidal decomposition of MTGCM thermospheric densities shows that observed ionospheric wave number 3 features are linked to a nonmigrating tidal mode with semidiurnal period ($\sigma = 2$) and zonal wave number 1 (s = −1) characteristics. The height of this photochemically determined ionospheric peak should be monitored regularly.   *INDEX TERMS:* 5435 Planetology: Solid Surface Planets: Ionospheres (2459); 5409 Planetology: Solid Surface Planets: Atmospheres—structure and dynamics; 6225 Planetology: Solar System Objects: Mars; *KEYWORDS:* ionosphere, Mars, thermosphere

1.   Introduction

1.1.   Background

[2]   Very few Mars thermosphere and ionosphere data sets presently exist to confirm the solar cycle, interannual, seasonal, dust storm and diurnal variations of the Mars upper atmosphere above 100 km. The temporal and spatial coverage afforded by spacecraft sampling of the Mars thermosphere and lower ionosphere to date is rather limited [cf. *Zhang et al.*, 1990; *Bougher et al.*, 2002]. Nevertheless, a concerted effort is presently being made to utilize available Mars Global Surveyor neutral and plasma data sets to systematically investigate thermosphere/ionosphere variations on solar to diurnal time scales.

[3]   The radio occultation technique can be used to probe the neutral and plasma structure of the Mars atmosphere. The Mars Global Surveyor (MGS) Radio Science (RS) experiment employs an ultrastable oscillator aboard the spacecraft that permits retrieval of neutral temperature profiles (0–50 km) as well as electron density profiles (~95–200 km), providing a means to monitor the characteristics of the Martian lower and upper atmospheres. Detailed analysis of the available neutral temperature profiles of the lower atmosphere is described in several recent papers [e.g., *Hinson et al.*, 1999, 2001, 2003a; *Hinson and Wilson*, 2002, 2004]. Corresponding electron density profiles are also beginning to be analyzed [*Bougher et al.*, 2001; *Mendillo et al.*, 2003; *Ness et al.*, 2003; *Krymskii et al.*, 2003]. These

[1]Space Physics Research Laboratory, University of Michigan, Ann Arbor, Michigan, USA.
[2]Lunar and Planetary Laboratory, University of Arizona, Tucson, Arizona, USA.
[3]Department of Electrical Engineering, Stanford University, Stanford, California, USA.
[4]Department of Astronomy, New Mexico State University, Las Cruces, New Mexico, USA.

electron density profiles are obtained at locations and during time periods often distinct from available accelerometer measurements of neutral thermospheric densities during aerobraking campaigns [*Keating et al.*, 1998; *Withers et al.*, 2003]. Clearly, the radio occultation profiles provide an opportunity to obtain high vertical resolution measurements of the Mars lower and upper atmosphere not possible otherwise.

[4] In a recent paper, *Bougher et al.* [2001] examined an initial set of RS electron density profiles obtained in late 1998 (24–31 December 1998), covering high northern latitudes (65–67N), early morning solar local times (SLT = 3–4), and high solar zenith angles (SZA = 78 to 81°). These 32-profiles covered a wide range of planetocentric longitudes with regular spacing about the planet. The height of the primary ionospheric peak was observed to have a mean during this aphelion season at this location of ~134.4 km. In addition, strong wave number 3 oscillations about this mean were clearly observed as a function of longitude. These oscillations appear to correspond to the background neutral density structure. Available neutral density variations measured by the MGS accelerometer experiment at the same latitude but slightly earlier during the Martian year show similar longitude variations. A mean ionospheric peak density of $8.1 \times 10^4 \, cm^{-3}$ was also observed during this RS sampling period, and was found to be comparable to values observed by the Mariner 9 extended mission radio occultation measurements, taken also during similar solar cycle (F10.7 = 130 at 1 AU), seasonal (~1.63–1.66 AU heliocentric distance), and SZA (70–80°) conditions [*Zhang et al.*, 1990].

[5] Analysis of these 32 MGS RS electron density profiles confirms that photochemical processes typically control the primary ionospheric peak height and magnitude [*Bougher et al.*, 2001]. Previous Martian ionospheric measurements and modeling exercises have shown that the dayside ionosphere below ~180 km is not subject to vertical or horizontal transport of ionization [e.g., *Zhang et al.*, 1990; *Fox*, 1997], but rather local photochemistry. Similarly, the mean RS ionospheric peak height observed in late 1998 is consistent with photochemical theory incorporating SZA and seasonal variations for Mars [*Stewart*, 1987; *Zhang et al.*, 1990]. Furthermore, the longitude variations of the peak height about this mean reflect underlying neutral density oscillations in the thermosphere. Together, these neutral and electron density variations appear to be an excellent indicator of the dynamical coupling of the Mars lower and upper atmospheres. In particular, nonmigrating tidal forcing is implicated by these high latitude ionospheric wave features [*Bougher et al.*, 2001]. These oscillations exhibit a longitude phasing similar to neutral density variations observed by the MGS accelerometer near 130 km [*Keating et al.*, 1998; *Withers et al.*, 2003], and temperature variations observed by the MGS Thermal Emission Spectrometer (TES) near 25 km [*Wilson*, 2000; *Banfield et al.*, 2003]. The propagation and impact of these tidal waves throughout the Martian lower and upper atmospheres is now being investigated by several modeling groups [*Forbes and Hagan*, 2000; *Forbes et al.*, 2002; *Wilson*, 2002; *Withers et al.*, 2003].

[6] This analysis of these RS electron density profiles confirms that the lower atmosphere indeed plays a role in elevating or lowering the thermosphere, thereby raising and lowering the ionospheric peak height. The peak height still occurs at optical depth unity, where peak absorption of EUV radiation by CO_2 molecules occurs. However, the altitude at which this occurs is pushed up or down on constant pressure surfaces as the thermosphere expands or contracts. This expansion and contraction of the Mars atmosphere is well known; i.e., it is the result of changing solar heating with the seasons and aerosol heating that varies with the passage of dust storms [e.g., *Zhang et al.*, 1990; *Wang and Nielsen*, 2003]. In addition, neutral density variations as a function of planetocentric longitude further modify the height of the ionospheric peak, giving rise to localized peaks and troughs in accord with photochemical theory [*Bougher et al.*, 2001]. These properties of ionospheric peak heights will be exploited in this paper to extend the sampling of the neutral upper atmosphere to unique observing periods outside aerobraking campaigns using new RS electron density profiles.

1.2. Objectives of This Paper

[7] A new suite of MGS RS electron density profiles is now present on the Stanford public Web site and available for study [*Hinson et al.*, 2003b]. In this paper, we present a new analysis of RS ionospheric peak heights gleaned from five separate RS data sets obtained over two Martian years. This temporal sampling affords us the opportunity to examine interannual variations of these ionospheric features and the underlying neutral thermospheric structure near aphelion conditions. Our primary goal is to interpret the mean and longitude variations of these peak heights in order to further quantify the coupling of the Mars lower and upper atmospheres. In addition, our studies seek to confirm the repeatability of the Mars thermospheric structure near aphelion conditions from one Mars year to the next. The present MGS RS profiles collected over just two Martian years cannot fully characterize this interannual variability. Nevertheless, Mars lower atmosphere observations over several Martian years [see *Clancy et al.*, 2000; *Liu et al.*, 2003; *Smith*, 2004] clearly demonstrate a repeatable pattern of aphelion temperatures that should be reflected aloft in thermospheric densities and ionospheric peak heights.

[8] The interpretation of these new RS electron density profiles will make use of a detailed three-dimensional (3-D) Mars thermospheric general circulation model (MTGCM) which incorporates a photochemical dayside ionosphere. The MTGCM simulates seasonal, SZA and longitude variations in the neutral density structure which will be reflected in the corresponding peak heights that are calculated. Matching of the observed RS and predicted MTGCM peak height variations enables us to extract the underlying SZA variation of the neutral thermospheric densities of the actual Martian thermosphere. The tidal processes responsible for maintaining the longitude variations of these peak heights will also be quantified by using the MTGCM code.

[9] In this paper, we will summarize the mean of the peak magnitudes extracted from the five MGS RS data sets (see Table 2). This provides a reference for comparison to MTGCM simulated values that will follow (in section 5). However, longitudinal variations of these peak magnitudes have been presented and discussed in detail elsewhere [*Ness et al.*, 2003; *Krymskii et al.*, 2003]. Peak magnitude varia-

Table 1. MGS/RS Data Set Parameters

Data Sets (Profiles)	Dates	Ls	SZA (LAT)
EDS1 (32)	24–31 December 1998	74–77	78–81 (64.7–67.3N)
EDS2 (43)	9–27 March 1999	108–116	76.5–77.8 (69.7–73.3N)
EDS3 (134)	9–21 December 2000	86.8–92.5	80.5–82.2 (67.5–69.6N)
EDS4 (220)	5–29 May 1999	134.7–146.3	78.6–86.9 (64.7–69.1S)
EDS5 (448)	9 Dec. 2000–31 Jan. 2001	86.8–110.9	75.3–82.2 (67.5–77.6N)

tions with longitude have been shown to be subject to crustal magnetic field influences. However, discussion in this paper is limited to peak height variations which the MTGCM is best suited to address. These separate investigations are consistent with the fact that different processes affect the longitude variations of Mars F1-peak heights and magnitudes.

[10] Section 2 describes the new RS data sets used for our investigations. Results from these five RS data sets are presented in section 3. A brief review of tidal theory, encompassing migrating and nonmigrating tides, and its application to the Mars upper atmosphere is given in section 4. MTGCM simulations of the thermospheric and ionospheric structure appropriate for near aphelion (northern hemisphere, late spring) conditions are presented in section 5 for interpreting the RS peak heights and their variations. Finally, conclusions are summarized in section 6.

2. Overview of New MGS Radio Science Data Sets

[11] The present analysis is carried out on five sets of MGS RS occultation measurements: (1) four obtained near northern summer solstice (Ls = 74–116, near aphelion) at high northern latitudes (64.7–77.6N), and (2) one set of profiles approaching equinox conditions (Ls = 135–146) at high southern latitudes (64.7–69.1S). Ls refers to the aerocentric longitude, which is an angular measure of the Martian seasons (Ls = 0 and 180 equinoxes; Ls = 90 northern summer solstice; Ls = 270 southern summer solstice). Electron density profiles over an altitude range of 95 to 200 km are examined for a modest range of solar zenith angles (75.3–86.9°) for local solar times of (1) 3–4 hours and (2) 12.1 hours. The planetocentric longitude separation between successive RS occultation tracks is typically about 55° (EDS1) and 28° (remaining RS data sets). Table 1 summarizes all RS data sets available for our present investigation and gives the dates and associated spatial/temporal parameters that enable these measurements to be used to address interannual ionospheric variations at Mars. In addition, Table 2 provides solar EUV

flux activity for each measurement period, with observed terrestrial fluxes (using the associated F10.7-cm index) scaled to the Mars orbit and properly rotated according to the specific solar elongation (see tables of *Espenak* [1994]). The simple lead or lag of the position of Mars relative to the Earth is utilized for this rotation. Tabulations of F10.7-cm fluxes are provided for both terrestrial and scaled Mars heliocentric conditions, in order to emphasize the net solar forcing at Mars for these RS sampling periods. Average ionospheric peak magnitudes and heights for each data set are given as a reference for later discussions regarding observed longitude variations.

[12] The examination of the interannual variations the MGS RS electron density profiles over 2 Martian years is a key objective of this paper. Table 1 indicates that only northern hemisphere data encompasses similar spatial and seasonal sampling over the 2 years. The southern hemisphere data set (EDS4) of year 1 has no counterpart in year 2. Thus the EDS4 data set will be analyzed but not included in the interannual discussions that will follow.

3. Electron Density Primary Peak Heights and Magnitudes

### 3.1. Northern Hemisphere, Season 1 (EDS1, EDS2)

[13] Two data sets (EDS1, EDS2) are available for aphelion season 1 (1998–1999) from RS occultations in the northern hemisphere (see Table 1). The number of electron density profiles represented is not large (75-total). However, the profiles from each data set span a very small range of SZA conditions. In addition, both of these data sets were taken close to solar moderate flux conditions at Mars (see Table 2). The combination of aphelion heliocentric distances and solar EUV fluxes (rotated from Earth to Mars) yields F10.7-cm fluxes at Mars that range over 41 to 59 units. RS profiles collected over nearly 3-weeks are examined to build up the longitude coverage to improve fitting statistics.

[14] Figure 1 shows that electron density peak heights (F1-peak heights) have a strong variation with longitude, with a mean height of ~134.4 km and local ridges or peaks

**Table 2.** MGS/RS Electron Density Peak: Mean Magnitudes and Heights[a]

Data Sets	Ne, 1/cm³	Height, km	Earth F10.7-cm flux	Mars F10.7-cm flux	Distance, AU
EDS1	8.1E + 04	134.4	132–181	46–55	1.67
EDS2	8.5E + 04	133.6	103–155	41–59	1.63
EDS3	7.5E + 04	134.8	126–201	43–59	1.66
EDS4	7.3E + 04	134.1–139.4	132–186	54–76	1.56
EDS5	8.5E + 04	133.8	126–202	47–75	1.64

[a]F10.7-cm fluxes at Mars: 25 (solar minimum, aphelion), 67 (solar moderate, average heliocentric distance), and 110 (solar maximum, perihelion). The F10.7-cm fluxes at Mars are properly rotated according to the solar elongation for the period (see tabulations of *Espenak* [1994]). Terrestrial F10.7-cm fluxes are not rotated, but taken directly from online data sets. Mean heights and magnitudes of the primary peak for each data set are tabulated. Read 8.1E + 04 as 8.1×10^4.
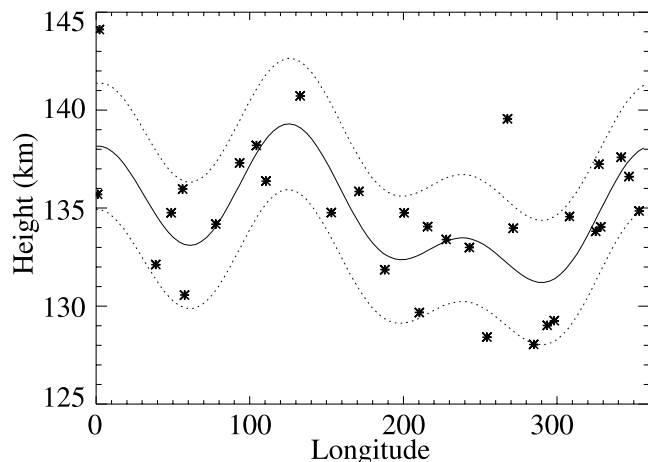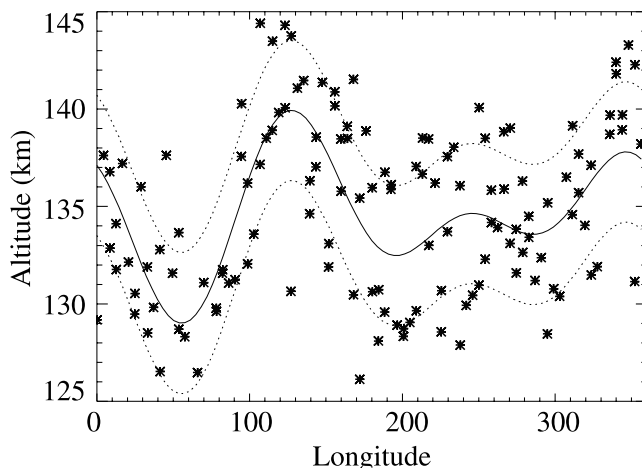
Figure 1. EDS1 data set. The heights of the primary electron density peak are presented as a function of longitude (season 1, aphelion). For this plot, a least squares wave number 1–3 spectral fit (solid curve) is applied to the RS data, with corresponding 1-σ errors (dotted curves) illustrated for this fit. The figure is revised from Figure 2a of *Bougher et al.* [2001]; a corrected 1-σ envelop is now displayed.

at 130 ± 10E and 0 ± 10E longitude [*Bougher et al.*, 2001]. (This plot is modified slightly from Figure 2a of *Bougher et al.* [2001]; i.e., 1-σ error bars are corrected and presented in Figure 1). Deviations from this mean height can reach ±4–7 km. The wave number 1–3 (waves 1, 2, plus 3) least squares fit reveals that wave number 2 and 3 features are predominant. A wave number 3 fit alone (not shown) has much larger 1-σ error bars. F1-peak magnitudes (see Table 2) have a mean of 8.1×10^4 cm^{-3}. Figure 2 demonstrates that the longitude coverage of the EDS2 data set is not complete. However, the mean F1-peak height (133.6 km) and magnitude (8.5×10^4 cm^{-3}) are reasonably close to EDS1 data set values. This is consistent with the
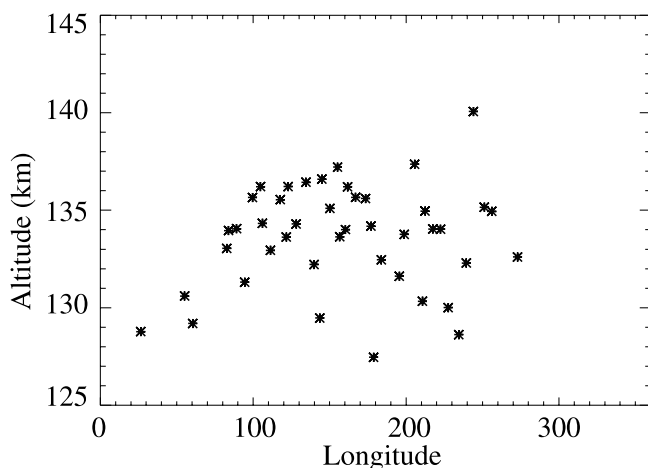
similar net solar flux, SZA, and seasonal conditions at Mars during the two observing periods. The longitude variation of F1-peak heights that is available (yet incomplete) for this EDS2 data set is still consistent with that of the earlier data set; i.e., peaks and troughs in the vicinity of 130E longitude appear to coincide. Aphelion season 1 (1998–1999) RS profiles are characterized by similar mean F1-peak heights and longitude specific variations that can be compared with corresponding features one Martian year later (2000–2001). This comparison specifically involves EDS1-2 (season 1) and EDS3 plus EDS5 (season 2) RS data sets.

### 3.2. Northern Hemisphere, Season 2 (EDS3, EDS5)

[15] Two data sets (EDS3, EDS5) are likewise available for aphelion season 2 (2000–2001) in the northern hemisphere (see Table 1). The EDS3 data set is a subset of the larger EDS5 data set (see Table 1). The former is composed of 134 electron density profiles collected near aphelion over a very small range of SZAs (80–82°) again during solar moderate conditions (F10.7-cm = 43–59 at Mars). These parameters are similar to those of RS profiles obtained 1 Martian year earlier (see Tables 1 and 2), enabling interannual comparisons to be made directly. On the other hand, the larger (EDS5) data set is composed of 448 electron density profiles also collected around aphelion conditions. However, the SZA range is much larger than for previous data sets (EDS1, EDS2, EDS3), requiring that SZA variations be considered before extracting longitude variations of F1-peak heights. EDS5 electron density profiles were also sampled over a wider range of solar fluxes affecting magnitudes (see Table 2).

[16] Season 2 F1-peak heights (Figure 3) exhibit a longitudinal variation that closely resembles the longitude pattern observed in season 1 (Figures 1 and 2). A mean height of ~134.8 km is now extracted with local ridges at

Figure 2. EDS2 data set. The heights of the primary electron density peak are presented as a function of longitude (season 1, aphelion). For this plot, a least squares spectral fit is not applied, since the longitude coverage for this sampling period is poor (not uniform).

Figure 3. EDS3 data set (subset of EDS5). This EDS3 data set covers a narrower range of SZA than the entire EDS5 data set, thereby minimizing SZA variations. The heights of the primary electron density peak are presented as a function of longitude (season 2, aphelion). For this plot, a least squares wave number 1–3 spectral fit (solid curve) is applied to the RS data, with corresponding 1-σ errors (dotted curves) illustrated for this fit.
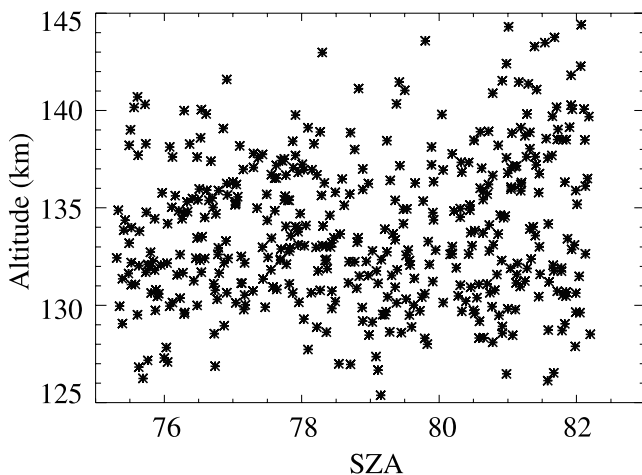
Figure 4. EDS5 data set. The heights of the primary electron density peak are presented as a function of SZA (season 2, aphelion). No clear trend of heights with SZA is apparent in this data set. This enables the entire EDS5 data set to be examined directly with no SZA correction. A total of 448 RS profiles is included.

130 ± 10E and 350 ± 10E longitude. These season 2 1-σ error bars (Figure 3) are comparable to those seen for season 1 (Figure 1). However, denser sampling for the EDS3 data set yields a clearer pattern of zonal variations. The wave number 1−3 least squares fit reveals that wave number 2 and 3 features are again predominant, with the wave-3 fit alone (not shown) yielding larger errors. In particular, the wave number 1−3 fit captures a strong ridge and its adjacent troughs near 130 ± 10E, with a trough-to-peak variation of at least 10 km. The corresponding F1-peak magnitudes (Table 2) have a mean of ∼7.5 × 10^4 cm^{-3}.

[17] As Table 1 shows, the season 2 EDS5 data set covers a larger range of SZA conditions (75−82°) than the previous EDS1, EDS2 and EDS3 data sets. Therefore SZA variations must first be extracted from the EDS5 electron density profiles before mean and longitude specific variations can be examined. Figure 4 illustrates the SZA variations of F1-peak heights for this EDS5 data set comprising 448 profiles. No clear trend of F1-peak heights with SZA emerges over this large sample of electron density profiles. Large solar zenith angle data with reduced electron densities may be somewhat noisier, thereby masking any real SZA trends in peak heights. For now, EDS5 F1-peak height variations can be examined directly and compared with previous season 1 behavior. Further discussion of SZA variations of peak heights and their implications for the underlying neutral atmosphere structure will be given in the context of new MTGCM simulations (see section 5).

[18] Figure 5 shows that season 2 (EDS5) F1-peak heights continue to have a persistent and strong variation with longitude, with a mean height of ∼133.8 km and prominent local ridges near 120 ± 10E and 350 ± 10E longitude. The wave number 1−3 least squares fit reveals that wave number 2 and 3 features are again predominant, similar to season 1. It is remarkable that ionospheric features, both the F1-peak mean height and longitude variations, are so similar during aphelion conditions one Martian year apart. This analysis implies that the Mars

lower and upper atmosphere structures are nearly the same for the 2 aphelion seasons covered by the MGS RS data sets. Available multiyear temperature data from the MGS TES instrument [*Liu et al.*, 2003; *Smith*, 2004] and ground-based microwave observations [*Clancy et al.*, 2000] near aphelion observing periods confirm the general repeatability of the Mars lower atmosphere structure from one Mars year to the next. Furthermore, larger scale dust storms that typically occur around perihelion do not have an impact on dust opacities near aphelion, which vary little from year to year [*Liu et al.*, 2003]. The new MGS RS observations of the Mars ionospheric structure presented in this paper are consistent with this lower atmosphere aphelion trend. However, it is not possible to extend this conclusion to all aphelion seasons without further upper atmosphere data.

3.3. Southern Hemisphere, Season 1 (EDS4)

[19] The EDS4 data set is obtained during northern hemisphere mid-summer conditions (Ls = 134.7−146.3) from RS occultations conducted in the southern hemisphere (see Table 1). This season 1 (1999) data set has no multi-Martian year counterpart, but it is useful for comparison to the previous data sets near aphelion conditions at smaller SZAs. The EDS4 data set is composed of 220 electron density profiles collected over a relatively large range of SZAs (78.6−86.9°) again during solar moderate conditions (F10.7-cm = 54−76) at Mars.

[20] Figure 6 illustrates the SZA variations of F1-peak heights for this EDS4 data set. Clearly, SZA variations must be taken into account before extracting longitude variations of F1-peak heights. The rise of F1-peak heights, and the decrease of the corresponding magnitudes, with increasing SZA is very characteristic of photochemical equilibrium conditions. The F1-peak heights require independent information about the background neutral atmospheric scale height near the F1-peak to perform a suitable correction for SZA variations [*Chamberlain and Hunten*, 1987; *Zhang et al.*, 1990]. For our studies, peak heights will be examined
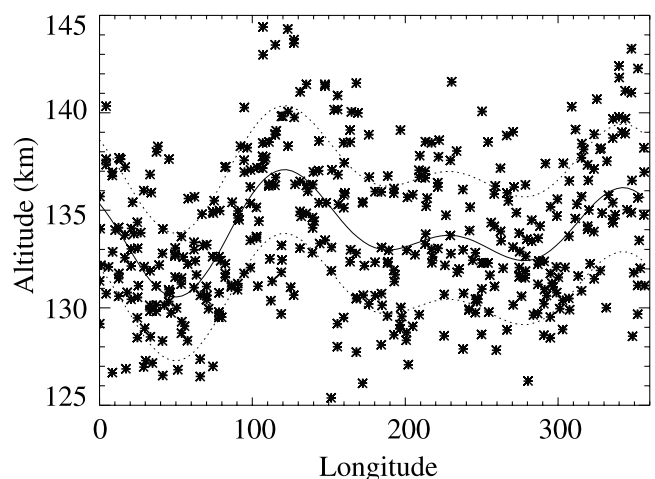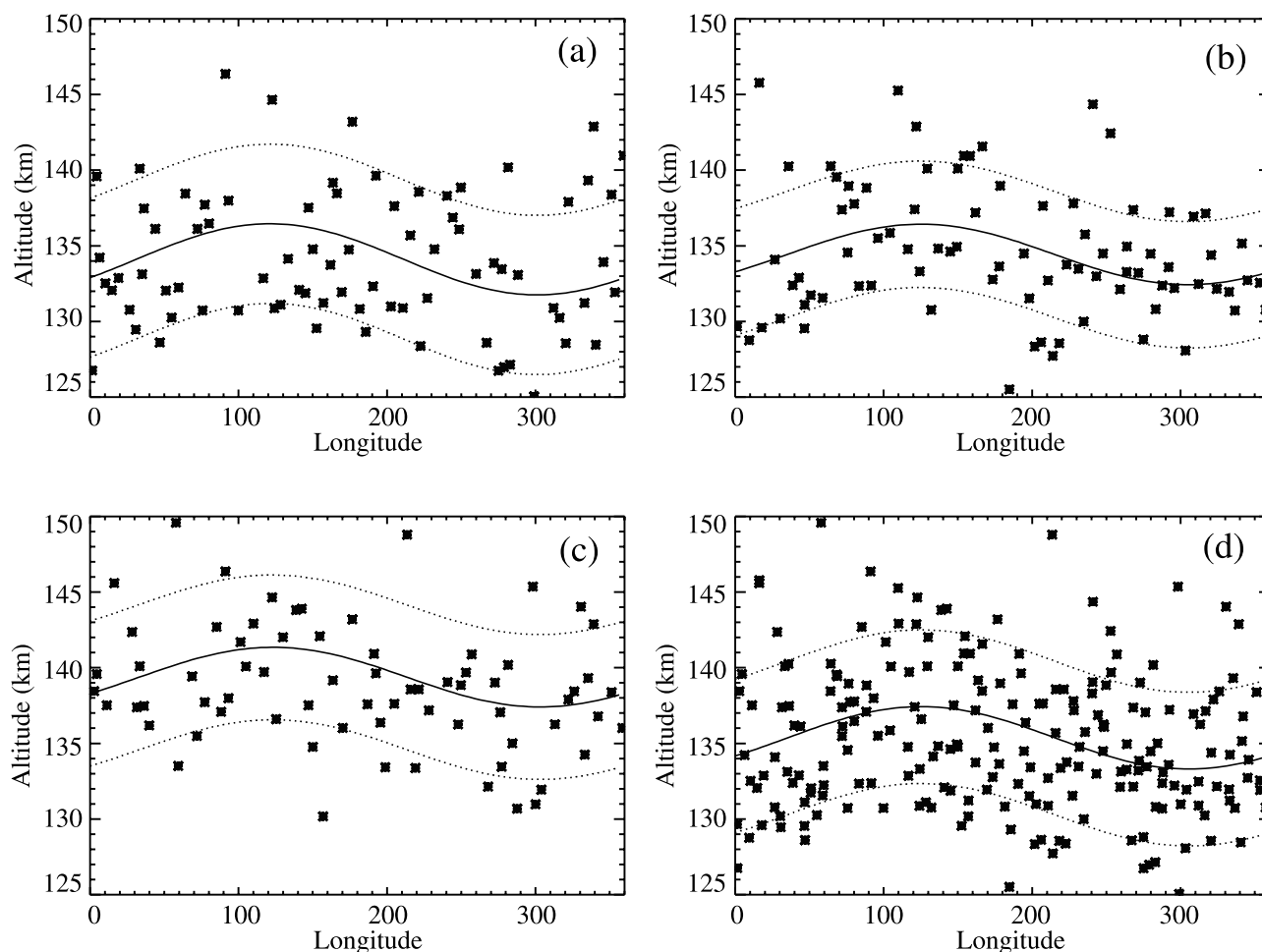

Figure 5. EDS5 data set. The heights of the primary electron density peak are presented as a function of longitude (season 2, aphelion). For this plot, a least squares wave number 1−3 spectral fit (solid curve) is applied to the RS data, with corresponding 1-σ errors (dotted curves) illustrated for this fit. A total of 448 RS profiles is included.
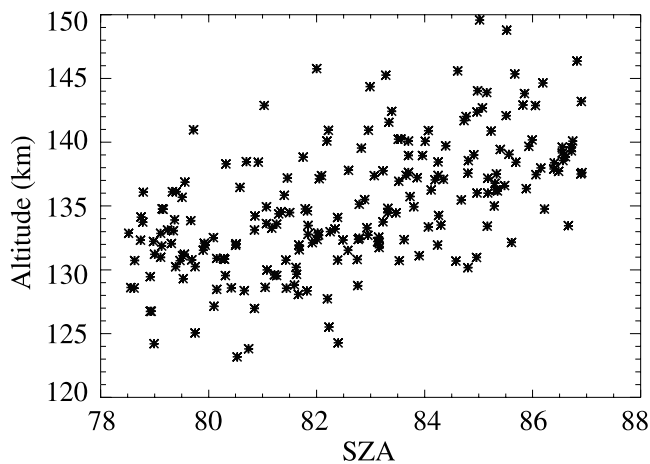
Figure 6. EDS4 data set. The heights of the primary electron density peak are presented as a function of SZA (season 1, northern mid-summer). Strong trends of these heights with SZA are visible, suggesting the partitioning of the entire data set into smaller SZA intervals is appropriate. A total of 220 RS profiles is included.

over smaller segments of the entire EDS4 data set, for which SZA variations are greatly reduced; i.e., (a) 78−81°, (b) 81− 84 °, and (c) 84−87° bins are chosen for this purpose.

[21] F1-peak heights over these three chosen EDS4 bins are examined, with a wave number 1 fit applied to the longitude variations that appear for each (Figures 7a−7c). In addition, a composite fit to the entire EDS4 data set (spanning SZA = 78−87°) is conducted and presented in Figure 7d. For the fitted segments and the composite, F1-peak heights exhibit a wave number 1 variation, with a ridge near 125 ± 25E and a corresponding trough near 305 ± 25E. The background mean height rises from (a) 134.1 km, to (b) 135.0 km, to (c) 139.4 km in conjunction with the increasing SZA conditions for each bin. Most importantly, the overall longitude pattern for each bin remains unchanged, with a composite mean F1-peak height of ∼136.0 km (see Figure 7d). The larger range of SZA conditions distinguish this data set from the others thus far examined in the northern hemisphere. The range of the F1-peak heights derived for this data set is larger than the range of the mean heights observed in the northern hemisphere. The most similar comparison of peak heights is found among data sets with

Figure 7. EDS4 data set. The heights of the primary electron density peak are presented as a function of longitude (season 1, northern mid-summer) for: (a) subset bin 1 (SZA = 78−81°), (b) subset bin 2 (SZA = 81−84°), (c) subset bin 3 (SZA = 84−87°), and (d) the entire EDS4 sample (SZA = 78−87°). For these plots, a least squares wave number 1 spectral fit (solid curve) is applied to the RS data, with corresponding 1-σ errors (dotted curves) illustrated for each fit.

similar SZA conditions (78–81°), which occurs for the EDS1 data set (134.4 km) and the early portion of the EDS4 data set (134.1 km). These data set comparisons confirm that SZA and seasonal conditions are important for controlling local Martian ionospheric peak heights on the dayside. Additional longitudinal variations are superimposed upon these well known SZA and seasonal trends.

[22] It is noteworthy to compare the differences in the longitude structures observed in the northern and the southern hemisphere data sets, both for high SZA conditions. Figures 1, 3, and 5 reveal a consistent wave number 2–3 pattern of longitude variations of the ionospheric peak heights for the northern hemisphere. Each of these data sets was obtained during local summer at early morning solar local times (SLT = 3–4). On the other hand, Figure 7d illustrates a southern hemisphere pattern of corresponding longitude variations for which wave number 1 features are predominant. This data set was obtained during winter conditions near local noon. It is possible that these differences reflect the role that seasonal and diurnal conditions have upon the successful vertical propagation of migrating and nonmigrating tidal modes up to thermospheric heights. Further discussion is given is section 4.

4. Brief Overview of Tidal Theory and Mars Applications

[23] Atmospheric tides are global-scale oscillations in temperature, wind, density, and pressure at periods which are harmonics of a solar or lunar day [Forbes, 1995]. The dominant forcing in the Martian atmosphere is solar heating by atmospheric and dust absorption. Both in situ thermally forced and upward propagating tides are thought to impact Martian altitudes above 100 km. If the excitation of such oscillations is nonuniform in longitude, then a Fourier series approximation of the zonal asymmetries can be derived for each atmospheric response field. Chapman and Lindzen [1970], Forbes and Hagan [2000], and others carefully outline the equations associated with these classical tidal oscillations. Mostly importantly, zonal wave number (s = ...−2, −1, 0, 1, 2...), temporal harmonic (σ = 0, 1, 2...), and phase (φ) parameters are commonly specified to identify the different tidal modes and their characteristics. For a diurnal tide, σ = 1; for a semidiurnal tide, σ = 2. Westward propagating tides have s > 0, eastward propagating tides have s < 0, and zonally-symmetric tides have s = 0. To an observer fixed on the planet, waves with s = σ migrate westward with the apparent motion of the sun; these oscillations are called "migrating tides". Waves with values of s ≠ σ travel faster or slower than the sun, or are standing (s = 0); these oscillations are called "nonmigrating tides". Much of the excitation for these nonmigrating tides on Mars is thought to occur as a result of nonlinear interactions between radiative processes and the surface, especially local topography. To first order, a longitudinal modulation of the westward-migrating tides is induced by the large scale topographic features of Mars [Zurek, 1976; Wilson and Hamilton, 1996; Forbes et al., 2002]. MGS accelerometer and RS observations were taken at nearly constant solar local time. In this context, the classical tidal equations demonstrate that the observed migrating tides become independent of longitude, while nonmigrating tides capture

the longitude dependence of the tidal oscillations [Forbes et al., 2002]. These nonmigrating tides now appear to be stationary with respect to the Mars surface with a zonal wave number of m = |s − σ|.

[24] Nonmigrating tidal components in the lower and upper atmospheres of Mars have received a great deal of attention since the advent of MGS TES and accelerometer data [e.g., Banfield et al., 2000, 2003; Forbes and Hagan, 2000; Wilson, 2002; Forbes et al., 2002; Withers et al., 2003]. The existence of significant longitude variations in the Mars thermospheric densities was first reported by Keating et al. [1998]. Later, detailed descriptions of these longitude features were given by Forbes et al. [2002] and Withers et al. [2003]. MGS accelerometer measurements of dayside thermospheric densities near 130 km revealed the presence of a ±22% wave number 3 component and a ±18% wave number 2 component throughout Phase 2 aerobraking over 50N to 60S latitude [Withers et al., 2003]. High northern latitude (60N) wave number 3 density oscillations were observed to be even larger. Subsequently, Bougher et al. [2001] observed the wave number 3 component again in the longitude variations of the RS electron density peak heights at 65–67N latitude (see section 1). It was proposed that this wave number 3 feature is due to an upward propagating nonmigrating tidal mode having σ = 2 (semidiurnal) and s = −1 (wave number 1, eastward propagating) characteristics [Bougher et al., 2001].

[25] This paper confirms the persistence of this wave number 3 feature in new RS data sets over 2-Mars years (see section 3). We now seek to quantify the nonmigrating tidal mode responsible for this wave number 3 feature by making use of new coupled MGCM-MTGCM simulations.

5. MTGCM Simulations and Interpretation of Northern Hemisphere Data Sets

5.1. Brief Summary of Coupled MGCM-MTGCM Codes Used

[26] The MTGCM itself is a finite difference primitive equation model that self-consistently solves for time-dependent neutral temperatures, neutral-ion densities, and three component neutral winds over the globe (see details given by Bougher et al. [1990, 1999a, 1999b, 2000, 2002, 2003]). Prognostic equations for the major neutral species (CO_2, CO, N_2, and O), selected minor neutral species (Ar, He and O_2), and several photochemically produced ions (e.g., O_2^+, CO_2^+, O^+, and NO^+ below 180 km) are included. These fields are simulated on 33 pressure levels (above 1.32 μbar), corresponding to ∼70–300 km (solar maximum conditions), with a 5° latitude and longitude resolution. The vertical coordinate is log-pressure, with a vertical spacing of 0.5 scale heights. Key adjustable parameters which can be varied for individual MTGCM cases include the F10.7 index (solar EUV/UV flux variation), the heliocentric distance and solar declination corresponding to the Mars seasons.

[27] The MTGCM is presently coupled to the NASA Ames Mars General Circulation Model (MGCM) code [e.g., Haberle et al., 1999] at the 1.32 μbar level, which falls in the altitude range of 60–80 km. This coupling allows both migrating and nonmigrating upward propagating tides to cross the MTGCM lower boundary and the effects of the
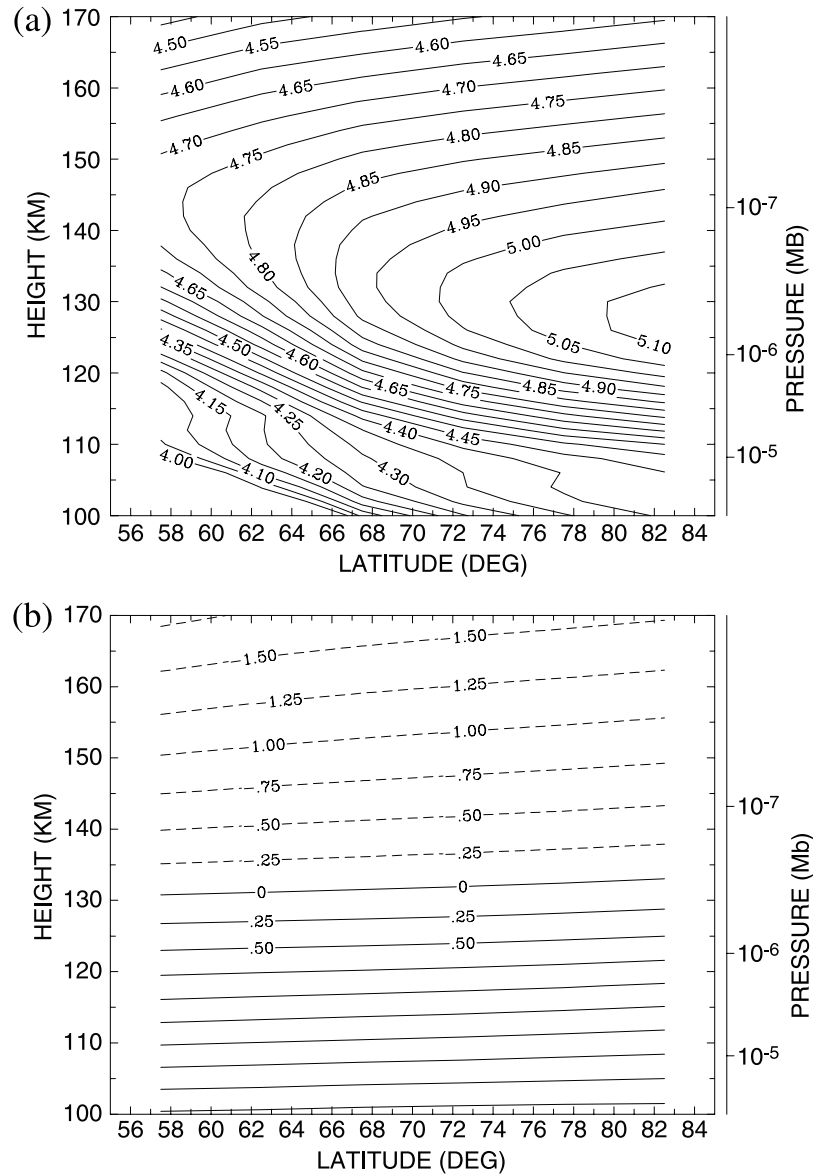
Figure 8. MGCM-MTGCM simulation for aphelion (Ls = 90) solar moderate flux conditions: (a) LOG10 electron densities (units of #/cm^3) and (b) LOG10 mass densities (units of kg/km^3). Both slices at SLT = 3 local time, illustrating the SZA behavior of the simulated primary peak magnitude and height, plus the underlying neutral density structure. Latitudes of 67.5 to 77.5N correspond to solar zenith angles of 82 to 74°.

thermal expansion and contraction of the Mars lower atmosphere to extend to the thermosphere. The entire atmospheric response to simulated dust storms can also be monitored using these coupled models. Key prognostic and diagnostic fields are passed upward from the MGCM to the MTGCM at the 1.32-microbar pressure surface at every MTGCM grid point: temperatures (T), zonal (U) and meridional (V) winds, and geopotential heights (Z). Two dimensional interpolation is applied to construct MGCM fields at 1.32-microbars that match the specific 5 × 5° MTGCM grid structure. No downward coupling from the MTGCM to the MGCM is presently activated. These two climate models are each run with a 2-minute time step, with the MGCM exchanging fields with the MTGCM at this frequency. Ten Martian day simulations are typically con-

ducted for various Mars seasonal and solar cycle conditions. Model histories are archived at 1- or 3-hour intervals throughout the Martian day, in order to capture the impact of longitude forcing upon time-dependent (specific local time) features throughout the integration. This coupled MGCM-MTGCM system has been validated using an assortment of spacecraft observations, including MGS Phase 1 and 2 aerobraking data [e.g., *Bougher et al.*, 1999b, 2003]. Assuming constant solar EUV fluxes, the MTGCM model cannot simulate interannual variability apart from interannual changes in the MGCM lower atmosphere dust opacities. The dust distribution and integrated vertical opacity can be simulated or specified according to recent MGS TES global data [see *Liu et al.*, 2003; *Smith*, 2004].

[28] At present, a simple photochemical ionosphere is formulated for the MTGCM including O_2^+, CO_2^+, O^+, and NO^+ below 180 km. Key ion-neutral reactions and rates are taken from *Fox et al.* [1995]; empirical electron and ion temperatures are adopted from the Viking mission. The ionization rates required for these production rates are calculated self-consistently making use of specified solar EUV fluxes. Photoelectron contributions to these ionization rates are parameterized within the MTGCM code.

[29] Aphelion season (Ls = 90) inputs are chosen for the coupled MGCM-MTGCM simulation presented in this paper. The scaled solar fluxes at Mars during aphelion solar moderate conditions are prescribed with an F10.7 = 47.0. The corresponding solar declination for northern summer on Mars is +25.0°. An MGCM visible dust opacity of 0.4 is implemented and assumed to be horizontally uniform over the globe. We compare the MTGCM simulations with the two years of MGS aphelion northern hemisphere data which is presented above in section 3. MTGCM plots are presented in section 5.2 that illustrate the longitude and SZA variations of the simulated electron density peak heights and magnitudes. Model comparisons to data are supplemented by the tidal decomposition of local neutral densities over thermospheric altitudes. This will enable the tidal fields responsible for the simulated longitude variations at high northern latitudes to be identified and their relative importance quantified as a function of altitude and latitude.

5.2. MGCM-MTGCM Coupled Model Results

[30] Figure 8a illustrates the latitude and altitude variations of MTGCM calculated electron densities at a constant solar local time of 3.0 hours (SLT = 3). A longitude of 225E is chosen for display, which is located midway between high northern latitude ridges and troughs of the MTGCM background neutral density structure (see Figure 9). Latitudes from 67.5 to 77.5N correspond to solar zenith angles from 82 to 74°, consistent with the SZA range of RS data sets acquired in the northern hemisphere (see Table 1).

[31] Photochemical control is clearly demonstrated as one observes the MTGCM electron density peak heights to rise from ∼130 to 134 km, and the peak magnitudes to decrease from ∼1.2 to 0.87×10^5 cm^{-3} with increasing SZA (74 to 82°). MTGCM calculated F1-peak heights (131−134 km) covering 78−82° SZA encompass those observed for the EDS1, EDS2, and EDS3 data sets, as well as for the mean SZA conditions of the EDS5 data set (see Table 2). This demonstrates that the coupled MGCM-MTGCM reliably reproduces the fundamental features of the neutral lower and upper atmospheres of Mars at aphelion conditions. The corresponding SZA variation of calculated thermospheric densities is illustrated in Figure 8b, revealing, a 33% decline of neutral densities at 135 km from SZA = 74 to 82°. This simulated SZA variation suggests that the Mars near terminator neutral densities at this location are declining toward the nightside at a rate less than required to keep up with the increase in the slant path. Therefore peak heights are rising with increasing SZA, unlike the situation over most of the Venus dayside [*Cravens et al.*, 1981]. Small model-data set differences do exist; i.e., the MTGCM calculated peak magnitudes are somewhat larger than observed (by 20−25%), and the corresponding average MTGCM peak heights are somewhat lower than observed (by ∼3.0 km) at the
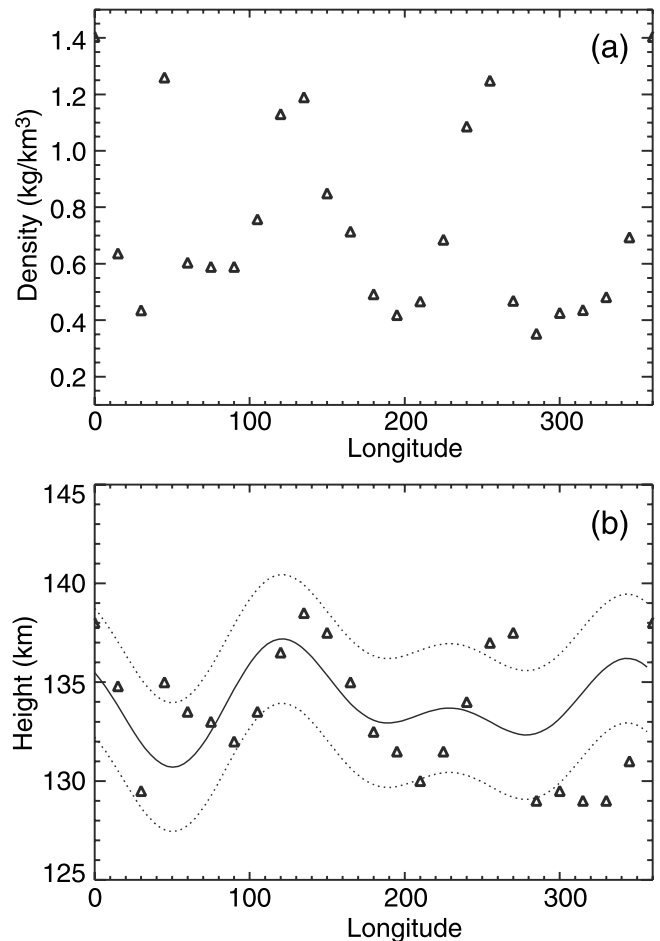
Figure 9. MGCM-MTGCM simulation for aphelion (Ls = 90) solar moderate flux conditions. Longitude variations of model generated (a) 133 km neutral densities (kg/km³), and (b) the heights of the primary electron density peak are presented for comparison. A wave number 3 oscillation appears for both simulated fields, yielding peaks and troughs in neutral densities and F1-peak heights that are in phase with one another over 62.5−77.5N. In addition, EDS1 and EDS5 northern hemisphere RS data sets are combined (480 profiles) to compare with the simulated heights (open triangles) in (b). For this panel, only the least squares wave number 1−3 spectral fit (solid curve) and the corresponding 1-σ errors (dotted curves) are presented for the observed RS data sets.

highest RS latitudes sampled. Historically, electron density peaks and altitudes were derived from radio occultation electron profiles obtained during the Mariner 9 extended mission [*Zhang et al.*, 1990]. For similar solar cycle, orbital, and SZA conditions, altitudes of 135 ± 5 km and densities of $0.75−1.2 \times 10^5$ cm^{-3} were observed. These values are consistent with the MTGCM predictions. Hence the reasonable match of this single MTGCM photochemical ionosphere simulation with RS observations over 2 Martian years provides a reference upper atmosphere model against which additional longitude variations of neutral densities and F1-peak heights can be studied.

[32] The averaged MTGCM neutral densities over 62.5−77.5N latitude are displayed in Figure 9a as a function of longitude at a constant solar local time (SLT = 3). These

longitude variations in total density are given at 133 km, close to the calculated mean ionospheric peak height. These density variations are produced by the interaction of in situ driven thermospheric densities and upward propagating nonmigrating tides captured by the coupled MGCM-MTGCM simulation [e.g., *Bougher et al.*, 2003; *Withers et al.*, 2003]. Neutral density ridges at these high northern latitudes are calculated at $0 \pm 20E$, $135 \pm 15E$, and $255 \pm 15E$ longitude; the largest of these is found at $0 \pm 20E$ longitude. The longitude phasing of these MTGCM density ridges reasonably matches that observed for season 1 and 2 RS electron density peak heights (see Figures 1, 3, and 5). The magnitudes of these simulated MTGCM density ridges and troughs have a standard deviation of ±43% about a mean of ~0.7 kg/km³. Assuming an atmospheric scale height of ~6.5–7.5 km, this implies the corresponding F1-peak heights should oscillate by ±3.0–3.5 km about a longitude mean value.

[33] Figure 9b illustrates the corresponding longitude variations of the averaged electron density peak heights for this same latitude band. A wave number 3 oscillation appears for these peak heights, yielding ridges and troughs that are in phase with MTGCM neutral densities over 62.5–77.5N latitude (see Figure 9a). The magnitudes of the MTGCM height variations (ridge-to-trough) are scattered about a mean value of 133.5 km with a standard deviation of ±3.4 km. Figure 9b also combines all the northern hemisphere RS observations (the rms fitted and 1-σ curves) and the MGCM-MTGCM calculated F1-peak heights for detailed comparison of longitude features. The ridge-to-trough height variations (MTGCM and RS data) are generally matched from 0E to 200E longitude, corresponding to the most prominent density ridges in Figure 9a. However, weaker longitude features in the observed RS peak heights, particularly near 210–270E longitude, are not well reproduced by the MGCM-MTGCM simulation.

[34] Finally, a wave number versus frequency decomposition of the MTGCM density field has been conducted (Figure 10a), revealing a prominent semidiurnal tidal response at high northern latitudes at 130 km. Simulated wave number 3 density features in fixed solar local time are clearly maintained by an eastward propagating, semidiurnal period ($\sigma = 2$) zonal wave number 1 (s = −1) tidal mode (long dashed curve) [*Bougher et al.*, 2001; *Wilson*, 2002; *Withers et al.*, 2003]. Current theory suggests that this wave number 1 nonmigrating tidal mode (hereafter indicated by SW1) arises from wave number 3 topographic modulation of the migrating semidiurnal tide [e.g., *Forbes et al.*, 2002]. *Banfield et al.* [2003] finds seemingly little evidence for this SW1 mode's presence at tropical latitudes in the Martian lower atmosphere thermal field during the time intervals covered by the RS data. Likewise, Figure 10a illustrates that this SW1 mode is much weaker in the MGCM-MTGCM simulation at lower latitudes (equatorward of 50 N). The migrating diurnal tide, generated by in situ solar EUV heating, is also important in the Martian thermosphere above ~125 km (solid curve). Figure 10b illustrates a latitude-height plot of the variation of the SW1 nonmigrating tidal mode amplitude with-respect-to the background mean, revealing fractional amplitudes of 0.15 to 0.30 over 110 to 160 km near 60–80N latitude. This plot should be compared with that of *Wilson* [2002] (see Figure 3c), whose
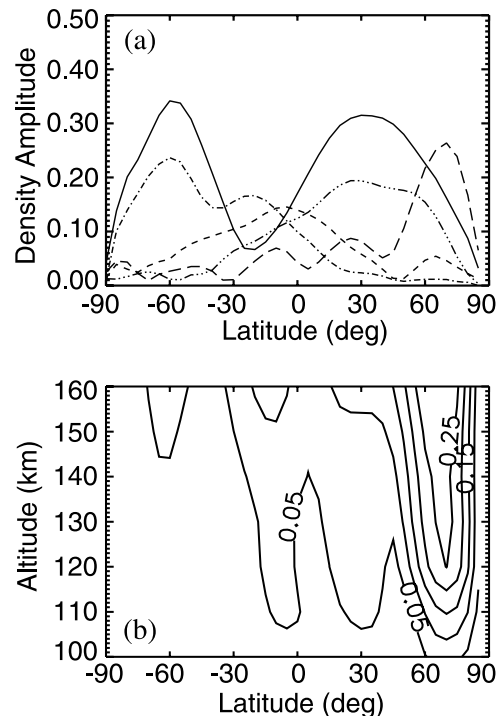
Figure 10. MGCM-MTGCM simulation for aphelion (Ls = 90) solar moderate flux conditions. (a) A frequency (σ)-wave number (s) decomposition of MTGCM densities at 130 km; fractional density amplitudes versus latitude are plotted for diurnal and semidiurnal (σ = 1 and 2) tidal modes having various wave numbers (s = −2, −1, 1, 2); (b) Latitude-height variation of the amplitude of the eastward propagating, semidiurnal period (σ = 2), zonal wave number 1 (s = −1) nonmigrating tide. Fractional density amplitudes are contoured. Attention is focused upon the features near 60–80N above 125 km where peak forcing is identified. Curves in (a) denote different tidal modes that are delineated as follows (σ, s): (2, −1) [long dashed], (1, 1) [solid], (1, −2) [3-dot dashed], (1, −1) [short dashed], and (2, 2) [dot dashed].

lower atmosphere GFDL MGCM model also predicted the importance of this same SW1 tidal mode specifically at these high northern latitudes in the Martian thermosphere. The present RS analysis further quantifies the importance of this nonmigrating tidal forcing upon the lower ionospheric structure at Mars.

[35] In conclusion, it is evident that wave number 3 longitude features exhibited in these MTGCM neutral densities near 130 km partially explain the corresponding variations in the observed F1-peak heights at these high northern latitudes. The impact of upward propagating nonmigrating tides upon thermospheric density variations and corresponding ionospheric peak heights is consistent with an expanded application of photochemical theory. Furthermore, the application of a global thermosphere model (MTGCM) with an embedded simple photochemical ionosphere is a valuable technique for interpreting these dayside RS electron density profiles below 180 km. General agreement between the simulated mean F1-peak heights, and their longitude variations, with several RS data sets is

obtained. However, the actual structure of the Mars neutral atmosphere and wave dynamics is not completely reproduced by this coupled MGCM-MTGCM simulation. An isolated semidiurnal period ($\sigma = 2$) zonal wave number 1 ($s = -1$) tidal mode is not sufficient to capture the wave number 2 and 3 longitude features observed. Furthermore, gravity wave impacts on atmospheric density variations are not addressed. In the future, the joint application of a detailed ionospheric model [e.g., *Fox*, 1997], a global model coupling both the small and large scale dynamics of the Mars lower and upper atmospheres [e.g., *Bougher et al.*, 2003; *Angelats-i-Coll et al.*, 2003], and a time-variable solar flux model [*Tobiska et al.*, 2000] is needed to systematically sort out the combined F1-peak height and magnitude variations in the Martian dayside ionosphere. Temporal (day-to-day, seasonal, solar cycle) and spatial (SZA, longitude) variations can then be addressed in great detail.

6. Summary and Conclusions

[36] Northern hemisphere MGS Radio Science electron density profiles taken over two Mars years at high latitudes (65–78N) provide a means to investigate the interannual variability of the Mars thermosphere/ionosphere during aphelion conditions. The primary ionospheric peak height varies with the background neutral atmosphere structure as a function of SZA and season, as expected according to photochemical theory. During 1998-1999 (aphelion season 1) and 2000–2001 (aphelion season 2), a repeatable longitude pattern is also observed in the high northern latitude ionospheric peak heights. A mean height of ~133.5–135 km is maintained over these two Martian years, with distinct local maxima occurring at $130 \pm 20E$ and $345 \pm 15E$ longitude. A pattern with prominent wave number 2 and 3 components is visible, and is consistent with upward propagating nonmigrating tides generated by modulation of migrating tides that interact with the large Martian topography [*Bougher et al.*, 2001; *Wilson*, 2002; *Forbes et al.*, 2002; *Withers et al.*, 2003]. This longitude pattern is superimposed upon the background SZA and seasonal trends in the ionosphere that are well known.

[37] It is remarkable that these ionospheric features, both the F1-peak mean height and longitude variations, are so similar during aphelion conditions one Martian year apart. The present analysis implies that the Mars lower and upper atmosphere structures are nearly the same for the 2 aphelion seasons covered by the MGS RS data sets. Available multiyear temperature data from the MGS TES instrument and ground-based microwave observations near aphelion observing periods confirm the general repeatability of the Mars lower atmosphere structure from one Mars year to the next. The new MGS RS profiles of the Mars ionospheric structure presented in this paper are consistent with this lower atmosphere aphelion trend. However, it is not possible to extend this conclusion to all aphelion seasons without further upper atmosphere data.

[38] Coupled MGCM-MTGCM simulations for these same aphelion and solar moderate conditions at Mars yield mean and longitude variable ionospheric peak heights, as well as mean ionospheric peak magnitudes, that reasonably match MGS RS observations. This correspondence indicates that the presently coupled MGCM-MTGCM models

do capture the basic atmospheric dynamics and fundamental photochemical processes controlling the Martian dayside ionosphere near 130 km. The MTGCM thus provides a reference model upper atmosphere against which additional longitude variations of neutral densities and F1-peak heights can be studied. A tidal decomposition of MTGCM thermospheric densities reveals wave number 3 features that are specifically linked to semidiurnal period ($\sigma = 2$) zonal wave number 1 ($s = -1$) tidal modes having the largest impact at/above 125 km. This pattern of electron peak heights is also largely consistent with the MGS accelerometer longitude pattern of neutral densities near 130 km.

[39] Finally, only one season (1998–1999) of electron density profiles is thus far available for the southern hemisphere (65–69S), now spanning a significant swath of SZA (78–87°). The observed variations in densities (decreasing) and heights (increasing) with increasing SZA confirm the strong photochemical control of the primary ionospheric peak heights and magnitudes. This is surprising since southern hemisphere crustal magnetic field structures are widespread and possess strong radial fields that should impact the ionospheric structure [*Ness et al.*, 2003; *Krymskii et al.*, 2003]. In addition, wave number 1 zonal variations in the ionospheric peak heights are observed, but are thus far unexplained.

[40] This paper demonstrates that the zonal variations of the Mars ionospheric peak heights first reported by *Bougher et al.* [2001] seem to be a persistent feature of the high latitude ionosphere near aphelion conditions. This ionospheric variability is in accord with the underlying neutral atmospheric structure. This fact should be exploited to expand our sampling of the Mars upper atmosphere. A long-term program for Mars thermosphere-ionosphere monitoring is needed to systematically investigate upper atmosphere variations on solar, seasonal, and diurnal time scales. The value of our present results, based upon a limited sampling of RS data, supports regular observations of ionospheric peak heights on the dayside of Mars. These data would provide an independent measure of the changing state of the Martian upper atmosphere.

References

Angelats-i-Coll, M., et al. (2003), Towards a global model of the Martian atmosphere (abstract), paper presented at International Workshop: Mars Atmosphere Modelling and Observations, Cent. Natl. d'Etudes Spatiales, Granada, Spain, 13–15 Jan.

Banfield, D., et al. (2000), Thermal tides and stationary waves on Mars as revealed by Mars Global Surveyor Thermal Emission Spectrometer, *J. Geophys. Res.*, *105*, 9521–9537.

Banfield, D., et al. (2003), Forced waves in the Martian atmosphere from MGS TES nadir data, *Icarus*, *161*, 319–345.

Bougher, S. W., R. G. Roble, E. C. Ridley, and R. E. Dickinson (1990), The Mars thermosphere: 2. General circulation with coupled dynamics and composition, *J. Geophys. Res.*, *95*, 14,811–14,827.

Bougher, S. W., S. Engel, R. G. Roble, and B. Foster (1999a), Comparative terrestrial planet thermospheres: 2. Solar cycle variation of global structure and winds at equinox, *J. Geophys. Res.*, *104*, 16,591–16,611.

Bougher, S. W., G. M. Keating, R. W. Zurek, J. M. Murphy, R. M. Haberle, J. Hollingsworth, and R. T. Clancy (1999b), Mars Global Surveyor aero-

braking: Atmospheric trends and model interpretation, *Adv. Space Res.*, 23(11), 1887–1897.

Bougher, S. W., S. Engel, R. G. Roble, and B. Foster (2000), Comparative terrestrial planet thermospheres: 3. Solar cycle variation of global structure and winds at solstices, *J. Geophys. Res.*, 105, 17,669–17,689.

Bougher, S. W., S. Engel, D. P. Hinson, and J. M. Forbes (2001), Mars Global Surveyor Radio Science electron density profiles: Neutral atmosphere implications, *Geophys. Res. Lett.*, 28, 3091–3094.

Bougher, S. W., et al. (2002), Simulations of the upper atmospheres of the terrestrial planets, in *Atmospheres in the Solar System: Comparative Aeronomy*, Geophys. Monogr. Ser., vol. 130, edited by M. Mendillo, A. Nagy, and H. Waite, pp. 261–288, AGU, Washington, D. C.

Bougher, S. W., S. Engel, and P. G. Withers (2003), The NCAR Mars thermospheric general circulation model: A review (abstract), paper presented at International Workshop: Mars Atmosphere Modelling and Observations, Cent. Natl. d'Etudes Spatiales, Granada, Spain, 13–15 Jan.

Chapman, S., and R. Lindzen (1970), *Atmospheric Tides: Thermal and Gravitational*, D. Reidel, Norwell, Mass.

Chamberlain, J. W., and D. M. Hunten (1987), *Theory of Planetary Atmospheres: An Introduction to Their Physics and Chemistry, Int. Geophys. Ser.*, vol. 36, 2nd ed., Academic, San Diego, Calif.

Clancy, R. T., et al. (2000), An intercomparison of ground-based millimeter, MGS TES and Viking atmospheric temperature measurements: Seasonal and interannual variability of temperatures and dust loading in the global Mars atmosphere, *J. Geophys. Res.*, 105, 9553–9571.

Cravens, T. E., A. J. Kliore, J. U. Kozyra, and A. F. Nagy (1981), The ionospheric peak on the Venus dayside, *J. Geophys. Res.*, 86, 11,323–11,329.

Espenak, F. (1994), *Twelve Year Planetary Ephemeris: 1995–2006, NASA Ref. Publ. 1349.*

Forbes, J. M. (1995), Tidal and planetary waves, in *The Upper Mesosphere and Lower Thermosphere: A Review of Experiment and Theory, Geophys. Monogr. Ser.*, vol. 87, edited by R. M. Johnson and T. L. Killeen, pp. 67–87, AGU, Washington, D. C.

Forbes, J. M., and M. Hagan (2000), Diurnal Kelvin wave in the atmosphere of Mars: Towards an understanding of 'stationary' density structures observed by the MGS accelerometer, *Geophys. Res. Lett.*, 27, 3563–3566.

Forbes, J. M., A. F. C. Bridger, M. E. Hagan, S. W. Bougher, J. L. Hollingsworth, G. M. Keating, and J. R. Murphy (2002), Nonmigrating tides in the thermosphere of Mars, *J. Geophys. Res.*, 107(E11), 5113, doi:10.1029/2001JE001582.

Fox, J. L. (1997), Upper limits to the outflow of ions at Mars: Implications for atmospheric evolution, *Geophys. Res. Lett.*, 24, 2901–2904.

Fox, J. L., P. Zhou, and S. W. Bougher (1995), The Martian thermosphere/ionosphere at high and low solar activities, *Adv. Space Res.*, 17(11), 203–218.

Haberle, R. M., et al. (1999), General circulation model simulations of the Mars Pathfinder atmospheric structure investigation/meteorology data, *J. Geophys. Res.*, 104, 8957–8974.

Hinson, D. P., and R. J. Wilson (2002), Transient eddies in the southern hemisphere of Mars, *Geophys. Res. Lett.*, 29(7), 1154, doi:10.1029/2001GL014103.

Hinson, D. P., and R. J. Wilson (2004), Temperature inversions, thermal tides, and water ice clouds in the Martian tropics, *J. Geophys. Res.*, 109(E1), E01002, doi:10.1029/2003JE002129.

Hinson, D. P., R. A. Simpson, J. D. Twicken, G. L. Tyler, and F. M. Flasar (1999), Initial results from radio occultation measurements with Mars Global Surveyor, *J. Geophys. Res.*, 104, 26,997–27,012.

Hinson, D. P., G. L. Tyler, J. L. Hollingsworth, and R. J. Wilson (2001), Radio occultation measurements of forced atmospheric waves on Mars, *J. Geophys. Res.*, 106, 1463–1480.

Hinson, D. P., R. J. Wilson, M. D. Smith, and B. J. Conrath (2003a), Stationary planetary waves in the atmosphere of Mars during southern winter, *J. Geophys. Res.*, 108(E1), 5004, doi:10.1029/2002JE001949.

Hinson, D. P., et. al. (2003b), Public access to MGS RS standard electron density profiles, Stanford Univ., Stanford, Calif. (Available at http://nova.stanford.edu/projects/mgs/eds-public.html)

Keating, G. M., et al. (1998), The structure of the upper atmosphere of Mars: In-situ accelerometer measurements from Mars Global Surveyor, *Science*, 279, 1672–1676.

Krymskii, A. M., T. K. Breus, N. F. Ness, D. Hinson, and D. I. Bojkov (2003), Effect of crustal magnetic fields on the near terminator ionosphere of Mars: Comparison of in situ magnetic field measurements with the data of radio science experiments on board Mars Global Surveyor, *J. Geophys. Res.*, 108(A12), 1431, doi:10.1029/2002JA009662.

Liu, J., J. M. I. Richardson, and R. J. Wilson (2003), An assessment of the global, seasonal, amd interannual spacecraft record of Martian climate in the thermal infrared, *J. Geophys. Res.*, 108(E8), 5089, doi:10.1029/2002JE001921.

Mendillo, M., S. Smith, J. Wroten, H. Rishbeth, and D. Hinson (2003), Simultaneous ionospheric variability on Earth and Mars, *J. Geophys. Res.*, 108(A12), 1432, doi:10.1029/2003JA009961.

Ness, N. F., et al. (2003), Characteristics of mini-magnetospheres formed by paleo-magnetic fields of Mars, in *Sixth International Conference on Mars* [CD-ROM], abstract 3119, Lunar and Planet. Inst., Houston, Tex.

Smith, M. D. (2004), Interannual variability in TES atmospheric observations of Mars during 1999-2003, *Icarus*, 167, 148–165.

Stewart, A. I. F. (1987), Revised time dependent model of the Martian atmosphere for use in orbit lifetime and sustenance studies, *LASP-JPL Internal Rep.*, NQ-802429, Jet Propul. Lab., Pasadena, Calif.

Tobiska, K., et al. (2000), The SOLAR2000 empirical solar irradiance model and forecast tool, *J. Atmos. Sol. Phys.*, 62, 1233–1250.

Wang, J.-S., and E. Nielsen (2003), Behavior of the Martian dayside electron density peak during global dust storms, *Planet. Space Sci.*, 51, 329–338.

Wilson, R. J. (2000), Evidence for diurnal period Kelvin waves in the Martian atmosphere from Mars Global Surveyor TES data, *Geophys. Res. Lett.*, 27, 3889–3892.

Wilson, R. J. (2002), Evidence for nonmigrating thermal tides in the Mars upper atmosphere from the Mars Global Surveyor Accelerometer Experiment, *Geophys. Res. Lett.*, 29(7), 1120, doi:10.1029/2001GL013975.

Wilson, R. J., and K. Hamilton (1996), Comprehensive model simulation of thermal tides in the Martian atmosphere, *J. Atmos. Sci.*, 53, 1290–1326.

Withers, P. G., S. W. Bougher, and G. M. Keating (2003), The effects of topographically-controlled thermal tides in the Martian upper atmosphere as seen by the MGS Accelerometer, *Icarus*, 164, 14–32.

Zhang, M. H. G., J. G. Luhmann, A. J. Kliore, and J. Kim (1990), A post-Pioneer Venus reassessment of the Martian dayside ionosphere as observed by radio occultation methods, *J. Geophys. Res.*, 95, 14,829–14,839.

Zurek, R. W. (1976), Diurnal tide in the Martian atmosphere, *J. Atmos. Sci.*, 33, 321–337.

————————

S. W. Bougher, Space Physics Research Laboratory, University of Michigan, Ann Arbor, MI 48109-2143, USA. (bougher@umich.edu)

S. Engel, Lunar and Planetary Laboratory, University of Arizona, Tucson, AZ 85721, USA. (sengel@lpl.arizona.edu)

D. P. Hinson, Department of Electrical Engineering, Stanford University, Stanford, CA 94305, USA. (hinson@rocc.stanford.edu)

J. R. Murphy, Department of Astronomy, New Mexico State University, Las Cruces, NM 88003, USA. (murphy@nmsu.edu)